JOURNAL OF PROPULSION AND POWER
Vol. 17, No. 2, March–April 2001

Oscillating Airfoil Aerodynamics of a Rotating Compressor Blade Row

Kuk Kim Frey* and Sanford Fleeter†
Purdue University, West Lafayette, Indiana 47907

Experiments are performed in a research compressor directed at investigating the aerodynamic damping unsteady aerodynamics of a rotor blade row. Specifically, the torsion mode unsteady aerodynamics of the first-stage rotor of a research compressor are investigated and quantified, including the effects of oscillation amplitude and steady aerodynamic loading. An experimental influence coefficient technique is implemented in conjunction with a unique torsion mode drive system that provides rotor blade torsion mode oscillations without other motor drive systems. The oscillating airfoil surface unsteady pressure influence coefficient data are acquired with dynamic pressure transducers embedded in the rotor blades. The resulting rotor blade aerodynamic damping oscillating airfoil data are then correlated with a linear theory prediction. In general, the unsteady pressure influence coefficient data decay rapidly with increasing distance from the reference blade, with different influences on the pressure and suction surfaces. Oscillation magnitude and steady loading have a significant effect on both the influence coefficient data and the equivalent all-airfoils-oscillating unsteady pressure data.

Nomenclature

$\bar{C}_p$	=	steady pressure coefficient
$\bar{C}_p^{n+}$	=	first harmonic unsteady pressure influence coefficient for nth blade oscillating
c	=	rotor blade chord
g	=	gravitational acceleration
l	=	length of cylindrical joint lever arm
n	=	rotor blade number or harmonic number
$\bar{P}$	=	rotor blade surface steady pressure
$\bar{P}_{e,c}$	=	corrected rotor blade exit midspan static pressure
p	=	time-variant rotor blade surface pressure
p^+	=	first harmonic unsteady pressure, psi
U	=	rotor blade midspan wheel speed
$\bar{V}_x$	=	mean axial velocity, determined by venturi orifice meter
$\bar{W}$	=	mean rotor inlet relative velocity
$\bar{y}$	=	half height of the cam follower rise
α'	=	time-variant rotor blade angular position
$\bar{\alpha}$	=	real-valued torsion oscillation magnitude or mean absolute flow angle
α^+	=	complex-valued torsion oscillation amplitude
ΔC_p^{n+}	=	first harmonic unsteady pressure difference influence coefficient for nth blade oscillating
ΔC_p^+	=	first harmonic unsteady pressure difference coefficient
$\Delta \bar{C}_p$	=	steady differential pressure coefficient
Δp^{n+}	=	reference blade first harmonic unsteady pressure difference for nth blade oscillation, psi
Δp^+	=	first harmonic unsteady pressure difference, psi
ρ	=	mean density of air
σ	=	interblade phase angle
ϕ	=	steady flow coefficient, $\bar{V}_x/U$
ω	=	rotor blade oscillation frequency or forcing function frequency, rad/s

Introduction

HIGH-CYCLE fatigue (HCF) of turbomachine blade rows is caused by flow-induced vibrations, with rotor blades particularly susceptible because of the large mean stresses from centrifugal forces. For flutter, a self-excited vibration, the unsteady aerodynamic forces acting on the blading are dependent only on the motion, that is, the blade displacement, velocity, and/or acceleration, with the flowfield supplying the energy to sustain that motion. Forced vibrations are externally excited blade vibrations in which the unsteady aerodynamic forces that cause the blade motion are independent of that motion.

The unsteady aerodynamics associated with flutter is analyzed by considering a harmonically oscillating cascade to determine the motion-induced unsteady aerodynamics or aerodynamic damping. With regard to forced response, the unsteady aerodynamic blade row response to a forcing function comprises two components: the gust response and the aerodynamic damping. With mechanical damping considerably reduced in advanced rotor designs, the aerodynamic damping determines the response level. Thus, it is important to investigate and quantify the motion-induced unsteady aerodynamics, the aerodynamic damping, for both flutter and flow-induced vibrations.

Unsteady aerodynamic modeling is continually improving, largely due to the rapid technological advancements in computing power and efficiency. However, the validity of the physical and mathematical assumptions inherent in these models, their limitations, and range of applicability have yet to be established. For the most part, new models are verified by correlating predictions with those of simpler models or with lightly loaded thin airfoil cascade data. This is due to the lack of appropriate data for model verification, to determine necessary enhancements to current models, and to direct the development of advanced ones. Also, the increased level of modeling from linearized analyses to Navier–Stokes methods is accompanied by the need for significantly increased computational resources. Thus, the establishment of the applicability and the limitations of the various models is also necessary to determine the most efficient analysis for a particular application.

Limited aerodynamic damping oscillating cascade data exists, with these experiments directed at flutter, even though these aerodynamic damping data are also of significance to forced response. This is due to the fundamental differences in aerodynamic damping for flutter and forced response. For flutter, the issue is stability, with the aerodynamic damping needed over the complete range of interblade phase angles, requiring extensive experimental time and complex and expensive airfoil drive systems. For forced response, vibration amplitude is key, with the aerodynamic damping required at a particular interblade phase angle valued at a frequency matching that of the forcing function.

Received 9 July 1998; revision received 30 June 2000; accepted for publication 14 August 2000.

*Research Assistant, School of Mechanical Engineering.
†McAlliste-Distinguished Professor, School of Mechanical Engineering.

The difficulty in oscillating a cascade of airfoils at a constant interblade angle has been overcome by an experimental influence coefficient technique.[1] The unsteady aerodynamics of the airfoil row oscillating at a constant interblade phase angle are obtained by means of influence coefficients in which only a single airfoil is oscillated, with the airfoil response measured on the oscillating airfoil and its stationary neighbors.

Linear cascades are, however, subject to endwall effects that can contaminate the oscillating cascade data.[2] Although able to be overcome, often with a great deal of effort, this difficulty is not present in a compressor blade row. Oscillating blade row unsteady aerodynamics was investigated in an isolated low-speed rotor, with the blades oscillated with a constant amplitude at different interblade phase angles.[3] However, even though the amplitude of oscillation was small, the correlation of these data with linear theory[4] was poor as a result of leading-edge separation that was not modeled.

Thus, it is important to investigate and quantify the motion-induced unsteady aerodynamics or aerodynamic damping of realistic airfoil configurations without endwall effects. For these unique data to be appropriate for both flutter and forced response model verification and direction, the effects of blade oscillation amplitude and steady loading over the complete interblade phase angle range must be considered.

This paper addresses these needs, describing experiments performed in a low-speed research compressor directed at investigating the aerodynamic damping unsteady aerodynamics of a rotor blade row. Specifically, the torsion mode unsteady aerodynamics of the first-stage rotor are investigated and quantified, including the effects of oscillation amplitude and steady aerodynamic loading. An experimental influence coefficient technique is implemented in conjunction with a unique torsion mode drive system that provides rotor blade torsion mode oscillations without other motor drive systems, that is, as long as the compressor is operating the mechanism oscillates a rotor blade. The oscillating airfoil surface unsteady pressure influence coefficient data are acquired with dynamic pressure transducers embedded in the rotor blade. The resulting oscillating airfoil data are then correlated with linear theory.

Experimental Influence Coefficient Technique

The unsteady aerodynamics of the blade row oscillating at a constant interblade phase angle is obtained by means of influence coefficients in which a single instrumented airfoil, $n = 0$, and its adjacent airfoils (Fig. 1) are individually oscillated. The influence of the nth blade oscillation is measured on the instrumented reference airfoil as an unsteady aerodynamic influence coefficient $\Delta C_p^{n+}(x)$. Then, Eq. (1) determines the unsteady aerodynamics of an equivalent blade row oscillating at a constant interblade phase angle σ. Because this influence coefficient technique involves the oscillation of a finite number of blades, the drive system cost and complexity are minimized. However, a disadvantage of this technique is the $2N - 1$ increase in experimental time required to individually oscillate each blade ($n = -N, \ldots, 0, \ldots, N$). Here,

$$\Delta C_p^{+}(x,\sigma) = \sum_{n=-N}^{N} \Delta C_p^{n+}(x) e^{in\sigma} \tag{1}$$

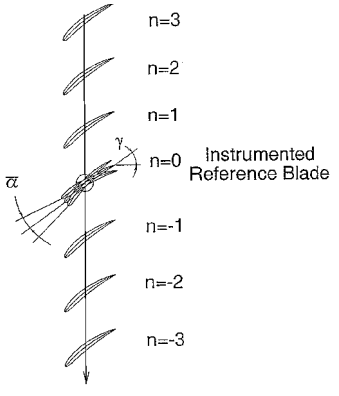

Fig. 1 Compressor blade row with instrumented oscillating reference blade.

Table 1 Airfoil and compressor characteristics

Airfoil type	Inlet guide vane	Rotor	Stator
Number of airfoils	36	43	31
Chord C, mm	30	30	30
Solidity	0.96	1.14	1.09
Camber Θ, deg	36.9	28.0	27.7
Stagger angle γ, deg	21.0	36.0	−36.0
Aspect ratio	2.0	2.0	2.0
Thickness/chord, %	10	10	10
Reynolds number, $\times 10^5$	6.3	6.3	5.0

Table 2 Additional rotor characteristics

Parameter	Value
Design flow rate, kg/s	2.03
Design axial velocity, m/s	24.38
Design rotational speed, rpm	2250
Number of stages	3
Design stage pressure ratio	1.0
Inlet tip diameter, mm	420.0
Hub/tip radius ratio	0.714
Stage efficiency, %	85

where $\Delta C_p^{+}(x,\sigma)$ and $\Delta C_p^{n+}(x)$ are the first harmonic unsteady pressure difference coefficient and influence coefficient for the nth rotor blade oscillating.

Research Compressor

The Purdue Axial Flow Research Compressor models the fundamental turbomachinery unsteady aerodynamic phenomena, including the incidence angle, the velocity and pressure variations, the reduced frequency, and the rotor and stator row geometries and flow conditions. The compressor is driven by a 15-hp dc electric motor at a speed of 2000 rpm. Each identical stage contains 43 rotor blades and 31 stator vanes having a British C4 airfoil profile. Table 1 presents the relevant compressor characteristics. Table 2 provides additional rotor characteristics.

Rotor Blade Oscillations

The rotor blade torsion mode drive system consists of three components: the blade assembly, the cam follower assembly, and the cam (Fig. 2). As the compressor rotates, the cam follower rides along the sinusoidal surface of a stationary cam, and its linear motion is translated into rotary motion via a lever arm fixed to the rotor blade. The elegance of this system is that the pitching motion of the rotor blades is achieved without employing any other motor drive systems: The mechanism oscillates the rotor blade as long as the compressor is operating. Also, the sinusoidal cam surface produces a single frequency harmonic motion.

The angular deflection amplitude for these experiments is 10-deg or less. Hence, the rotor blade torsion motion $\alpha'(t)$ is

$$\alpha'(t) \cong (\bar{y}/l)\sin\omega t = \bar{\alpha}\sin\omega t \tag{2}$$

Because four rotor blades are instrumented with dynamic pressure transducers, rotor blades designated $n = -2, -1, 0$, and 1 are individually oscillated (Fig. 3). This is accomplished with four identical mechanisms operated simultaneously. Individual blade oscillations are accomplished by indexing the endplate with the cam follower assemblies to the appropriate blades. First, the inner parts of the rotor blade assembly are indexed to the particular blades to be oscillated. Then, the plate is engaged by rotating the endplate until the cylindrical joint slips onto the cam follower shaft slot. Cams with different vertical heights vary the torsion mode amplitude.

Instrumentation and Data Acquisition

The instantaneous motion of the oscillating rotor blades $\alpha'(t)$ is determined by a precision rotary potentiometer with voltage output linearly proportional to angular position. These data are accurate to within 0.15 deg.

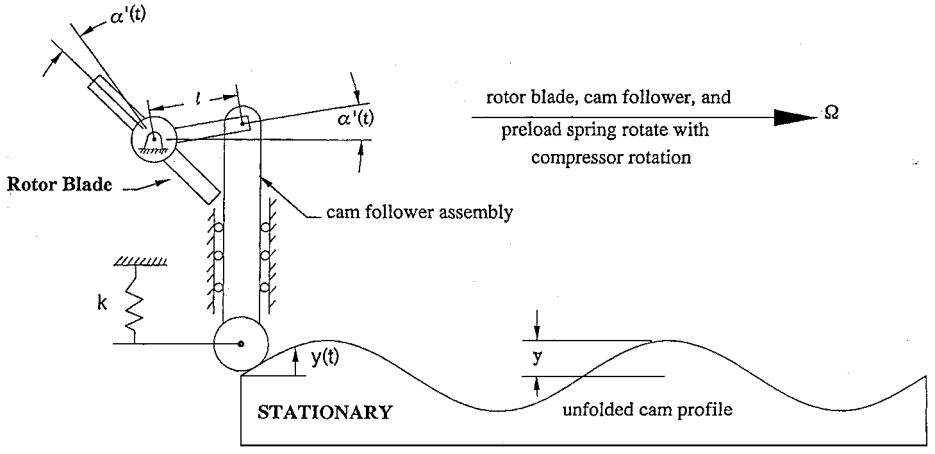

Fig. 2 Schematic of rotor blade oscillation mechanism.

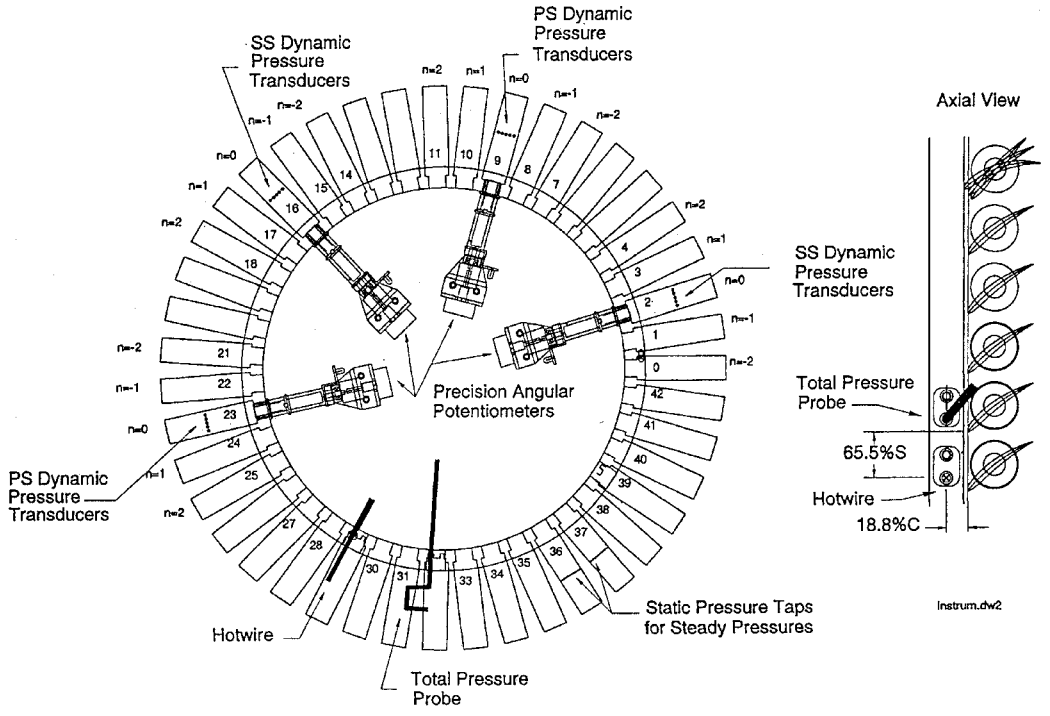

Fig. 3 Rotor instrumentation.

The inlet flowfield to the first-stage rotor is measured with a rotating cross hot wire mounted at blade midspan, 18.8% chord upstream of the blade leading edge and 65.5% span circumferentially from an adjacent rotor blade. The hot wire is calibrated for velocities ranging from 100 ft/s (30.5 m/s) to 200 ft/s (61.0 m/s) and flow angles ranging from −40 to +40 deg, with the velocity and flow angle uncertainty estimated to be 5% and ±0.5 deg.

The first-stage rotor blade steady aerodynamic loading is obtained with a rotor-based Scanivalve transducer system. Two blades are instrumented with 10 midspan static pressure taps, one pressure surface, and one suction surface. The rotor blade unsteady aerodynamics is obtained with 20 ultraminiature high-response pressure transducers installed at midspan on four blades. These transducers can operate to 10,000 g steady acceleration and 100 g of 2-kHz dynamic acceleration. Thus, the transducers are suitable for the steady rotating (1018 g) and dynamic (50 g at 66.67 Hz) environments of these experiments. To minimize the possibility of flow disturbances associated with the inability of the transducer diaphragm to maintain exactly the surface curvature of the blade, a reverse mounting technique is utilized. The transducers are calibrated statically and dynamically, with the static calibration uncertainty estimated to be ±4%. Dynamic calibration for frequencies ranging from 40 to 2700 Hz revealed a maximum gain and phase error of ±0.60 dB and ±1.5 deg.

A computer-controlled digital data acquisition and analysis system is based on the detailed instrumentation shown in Fig. 3. The rotor-based steady and unsteady data are transmitted to the stationary reference frame through a mercury-wetted slip ring. Low noise to signal ratio is achieved by amplifying the low-amplitude dynamic pressure voltages 200 times.

The steady data are determined by averaging 100 samples of the Scanivalve pressure signals and 200 samples of the hot-wire signals. Uncertainties in the mean values are calculated from the Student-t 95% confidence distribution. The time-variant cross hot wires and dynamic pressure transducer signals are remotely multiplexed and then amplified before being digitized. An optical trigger mounted on the compressor shaft controls the acquisition of the time-variant signals.

The rotor blade loading is characterized by a steady pressure coefficient $\bar{C}_p(x)$:

$$\bar{C}_p(x) = [\bar{P}(x) - \bar{P}_{e,c}]/\rho \bar{W}^2_{\text{adj}} \tag{3}$$

where $\bar{P}(x)$ is the rotor blade surface steady pressure, $\bar{P}_{e,c}$ is the corrected rotor blade exit static pressure for midspan, and $\bar{W}_{\text{adj}}$ is the mean rotor inlet relative velocity adjusted for the rotor blade potential field.

The rotor blade torsion mode unsteady aerodynamics are characterized by the unsteady pressure influence coefficients [Eqs. (4) and (5)] and the equivalent all-blades-oscillating unsteady pressure coefficients [Eqs. (6–8)]:

$$C_p^{n+}(x) = p^{n+}(x)/\rho\bar{W}^2\alpha^+ \tag{4}$$

$$\Delta p^{n+}(x) = p_{ss}^{n+}(x) - p_{ps}^{n+}(x) \tag{5}$$

where p^{n+} is the reference blade first harmonic unsteady pressure influence for the nth blade oscillating and $\rho\bar{W}^2$ is the mean rotor relative dynamic pressure. Hence,

$$\Delta C_p^{n+}(x) = C_{ss}^{n+}(x) - C_{ps}^{n+}(x) \tag{6}$$

$$C_p^+(x,\sigma) = \sum_{n=-N}^{N} C_p^{n+}(x)e^{in\sigma} \tag{7}$$

$$\Delta C_p^+(x,\sigma) = \sum_{n=-N}^{N} \Delta C_p^{n+}(x)e^{in\sigma} \tag{8}$$

where C_p^+ is the first harmonic unsteady pressure coefficient.

The first harmonic unsteady lift and moment coefficients are determined from the rotor blade surface unsteady pressure differences:

$$C_{l^*}^+ = \frac{1}{\Delta c}\int_{5.5\%c}^{81.0\%c} \Delta C_{p^*}^+ \, dx$$

$$C_{m^*}^+ = \frac{1}{(\Delta c)^2}\int_{5.5\%c}^{81.0\%c} \Delta C_{p*}^+(x_{ea} - x)\, dx \tag{9}$$

where

$$\Delta C_{p^*}^+ = \frac{P_{ss}^+ - P_{ps}^+}{\rho\bar{W}^2(\alpha^+/\bar{\alpha})}$$

and $\Delta c = 81.0\%c - 5.5\%c$.

Results

Experiments are performed in a research compressor directed at investigating and quantifying the aerodynamic damping unsteady aerodynamics of the first-stage rotor, including the effects of oscillation amplitude and steady aerodynamic loading. The resulting steady and unsteady aerodynamic data are correlated with linear theory predictions.

Steady Pressure Data

The effect of steady loading on the rotor blade surface steady pressure distribution is shown in Fig. 4. Also presented are predictions from the incompressible inviscid small camber airfoil cascade analysis INCMCSCD.[5]

The steady pressure distribution is a function of the steady loading only, as defined by the mean flow incidence angle or flow coefficient. The steady pressure on both rotor blade surfaces is affected by the loading level predominantly in the front half chord region, with the pressure surface steady pressure increased and the suction surface steady pressure decreased in this region. Increased steady loading results in increased steady pressure difference over the entire airfoil, particularly in the front half chord region. Overall, these steady data agree well with the INCMCSCD predictions, except in the leading-edge region, where the steady pressure gradient correlation is poor. The INCMCSCD analysis correctly predicts the chordwise location of the maximum pressure difference at the low steady loading level, but not at the high steady loading level. The correlation at the high steady loading level is not as good.

Rotor Blade Torsion Motion

Figure 5 shows the 10-deg oscillation amplitude high steady loading airfoil motion imparted to the four instrumented rotor blades by the drive system. The drive system imparts a predominantly first harmonic torsion mode oscillation to the rotor blades, with the second harmonic less than 3.5% and the third harmonic less than 10.7% of the first harmonic.

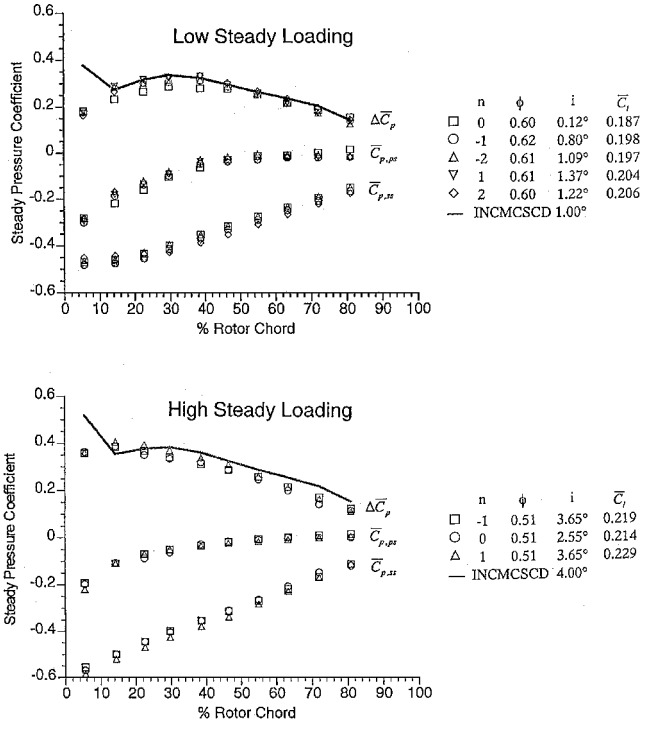

Fig. 4 Rotor blade surface steady pressure distributions.

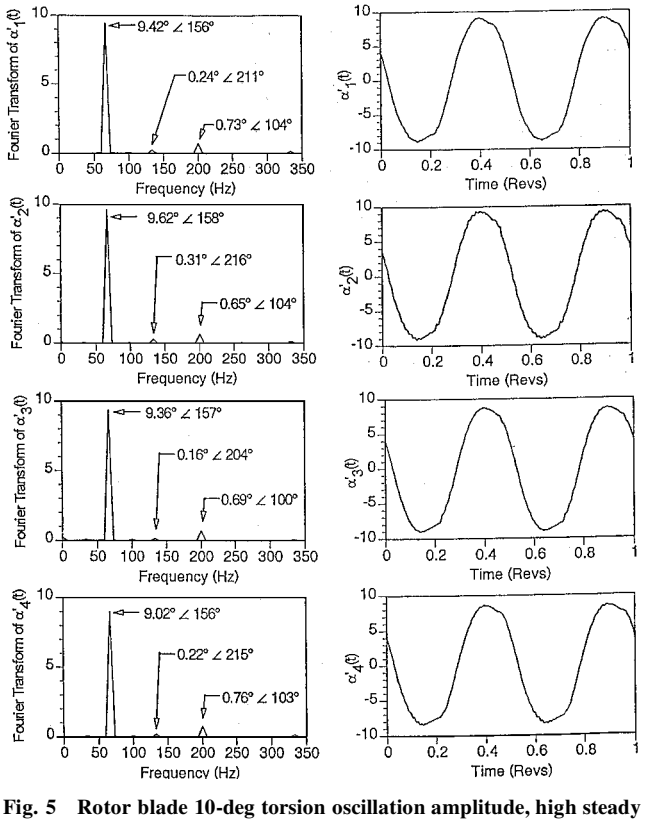

Fig. 5 Rotor blade 10-deg torsion oscillation amplitude, high steady loading.

First Harmonic Influence Coefficients

Figure 6 shows the effect of oscillating blade position on the reference blade suction surface unsteady pressure influence coefficients for oscillating blades in position from $n = -2$ to $+1$. In general, the aerodynamic influence of the oscillating blade decays rapidly

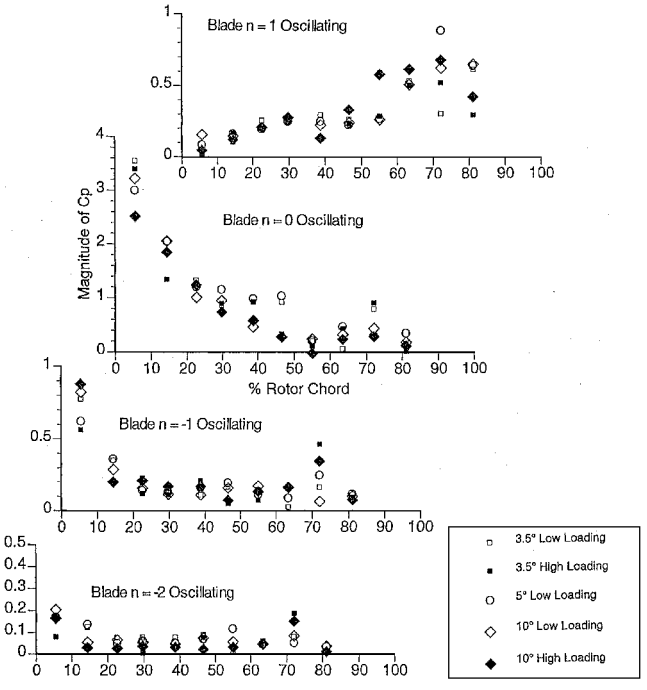

Fig. 6 Oscillating blade position effect on suction surface influence coefficient magnitude.

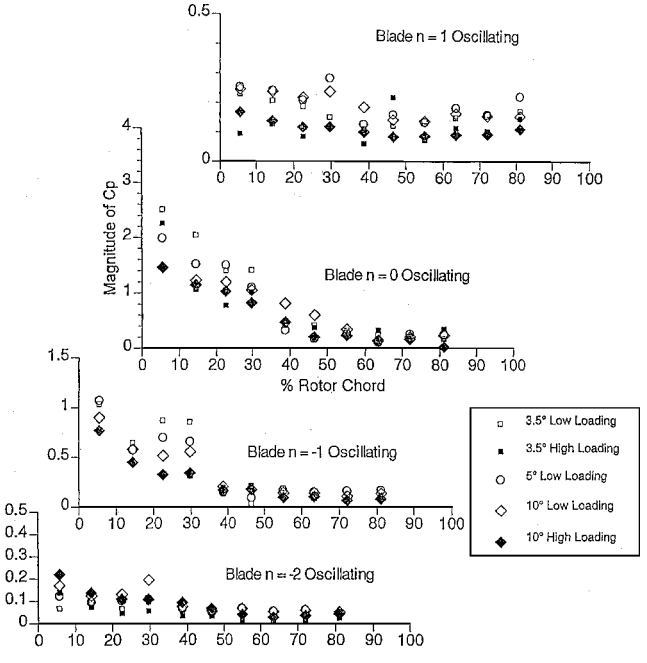

Fig. 7 Oscillating blade position effect on pressure surface influence coefficient magnitude.

with increasing distance from the reference blade. The $n = -1$ and $+1$ blades generate aerodynamic influences of the same magnitude on the reference blade, but affect different chordwise regions. The $n = -1$ blade oscillation affects the reference blade leading-edge region, whereas the $n = 1$ blade oscillation influences the trailing-edge region. This is due to the $n = -1$ blade being closer to the reference blade leading edge, whereas the $n = +1$ blade is nearer to the trailing-edge region. Also, there are strong effects of both oscillation amplitude and steady loading on the $n = 0$ reference blade self-influence pressure coefficient data. However, the effects of torsion oscillation amplitude are smaller than those of steady loading when the blades adjacent to the reference blade are oscillating.

The effect of blades in position from $n = -2$ to $+1$ oscillating on the reference blade pressure surface influence coefficients is presented in Fig. 7. The reference blade pressure surface data decrease

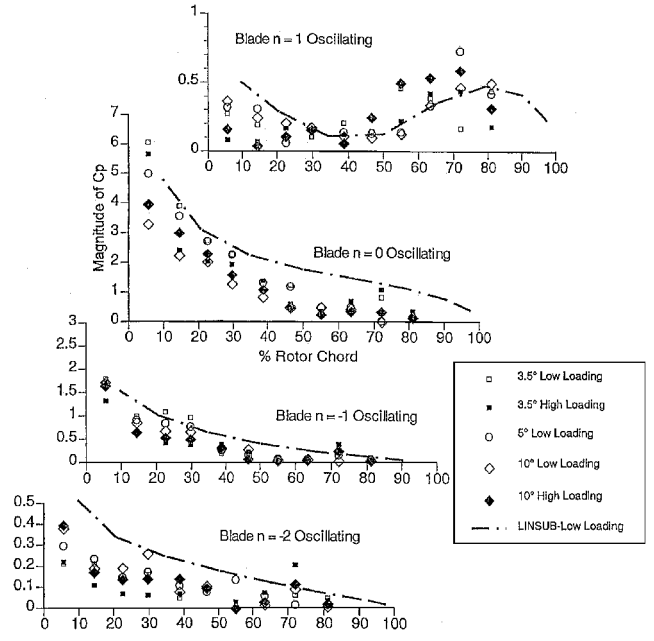

Fig. 8 Oscillating blade position effect on unsteady pressure difference influence coefficient magnitude.

in magnitude with increasing distance from the reference blade, but less rapidly than on the suction surface. The oscillation amplitude has a greater influence on the pressure surface than on the suction surface. Also, steady loading effects are prevalent on the reference blade for each oscillating blade position.

Figure 8 shows the effect of oscillating blade position on the reference blade unsteady pressure difference influence coefficients. These reference blade data are affected differently by oscillating blades in different positions. In general, the pressure difference influence is largest for the $n = 0$ reference blade self-influence data, with the influence rapidly decreasing with increased distance between the oscillating rotor blade and the reference blade. The effects of oscillation amplitude are large with the reference blade oscillating, but smaller for other blades oscillating. However, steady loading effects are evident for each blade oscillating.

Also presented in Fig. 8 are predictions of the unsteady pressure difference influence coefficients determined from LINSUB, a compressible flat plate cascade analysis.[6] The reference blade unsteady pressure difference influence coefficients correlate relatively well with LINSUB for blades $n = 0$, 1, and -1, but not as well for $n = -2$. Note the improved correlation at low steady loading levels. In addition, the correlation is better for the lowest amplitude of oscillation, 3.5 deg, especially in the front half chord region for blade $n = 0$ oscillating. This is due to the stagger angle input to LINSUB matching the inlet flow angle and the low oscillation amplitude best matching the assumptions of LINSUB, that is, small perturbations and low steady loading. The correlation is poorer in the aft chord region for blade $n = 0$ oscillating because camber and steady loading effects are present and not accounted for by LINSUB and because the analysis stagger angle no longer matches the local real blade flow angle.

Equivalent All Airfoils Oscillating Unsteady Aerodynamics

The number of blades to be oscillated to obtain equivalent all-airfoil-oscillating data per Eq. (1) was experimentally investigated. As shown in Fig. 9, the unsteady lift requires four terms, including the $n = -2$ to $+1$ blade oscillations to define the five-term $n = -2$ to $+2$ summation within 0.6% and 3-deg phase shift for the 10∞ case and within 1.7% and 1-deg phase shift for the 5-deg oscillation amplitude. However, the unsteady moment coefficient is closest to the five-term summation with only three blades oscillating in position from $n = -1$ to $+1$. The three-term summation magnitude is within 0.23% with less than 9-deg phase shift for the 10-deg oscillation amplitude and within 1.1% with 7-deg phase shift for the 5-deg

oscillation amplitude. The primary reason for the $n = 2$ blade having such a reduced effect on the overall unsteady aerodynamics is that the aerodynamic influence from blades above the reference airfoil, $n = 1$ and 2, is largely over the aft portion of the reference airfoil, where the unsteady pressures are of low magnitude. Conversely, the aerodynamic influence of blades oscillating in positions below the reference airfoil is largely over the leading-edge region, where the unsteady aerodynamic pressures are large. Thus, in these experiments, only blades from $n = -2$ to $+1$ were individually oscillated.

Equivalent All-Airfoils-Oscillating First Harmonic Data

Figures 10 and 11 show the effect of oscillation amplitude and steady loading on the suction surface, pressure surface, and pressure difference magnitude and the phase data for the equivalent rotor row with all blades oscillating for an interblade phase angle of -16.74 deg and reduced frequency $k = 0.282$ at low steady loading and $k = 0.290$ at high steady loading level.

There is a pronounced effect of oscillating amplitude on the pressure surface unsteady pressure. Namely, a region of large unsteady pressure is evident over the front half of the rotor blade, whose size is largely dependent on oscillation amplitude. At the 3.5-deg oscillation amplitude, the region of large unsteady pressure occurs over the front 20% chord followed by a region of reduced unsteady pressure over the next 20% chord. A 5-deg oscillation amplitude extends this region to 40% chord, and a 10-deg oscillation amplitude extends this region farther to 55% chord. At all three oscillation amplitudes, the pressure surface unsteady pressure is small and relatively constant beyond this region (Fig. 11). Steady loading reduces the region of large unsteady pressure. The oscillation amplitude affects the unsteady pressure phase when the value is changed from 3.5 to 5 deg, with no effect when the oscillating amplitude is increased to 10 deg. Increased steady loading causes a large phase response over the aft chord region.

Both the oscillation amplitude and the steady loading affect the entire suction surface, but these effects are smaller than on the pressure surface. In the leading-edge region, the unsteady pressure decreases with increased oscillation amplitude and increased steady loading. Over the front 20% chord, steady loading has a larger effect on the unsteady pressure magnitude than oscillation amplitude. However, oscillation amplitude effects dominate in the midchord region. Here the unsteady pressure decreases, with the decrease being more rapid with increased oscillation amplitude. The minimum unsteady pressure occurs at 72% chord for 3.5-deg, 65% chord for 5-deg oscillation amplitude and 40% chord for 10-deg oscillation amplitude at low steady loading. The effect of steady loading on this minimum is mixed. Large effects of oscillation amplitude on the suction surface phase data are evident, with a large shift in suction surface phase occurring earlier across the chord with increased oscillation magnitude. In contrast, steady loading delays the onset of the sudden suction surface phase shift.

With regard to the unsteady pressure difference, the effects of oscillation amplitude and steady loading seen on the individual airfoil surfaces are manifest. The primary effect of increased oscillation amplitude is to decrease the unsteady pressure difference in the leading-edge region. Increased oscillation amplitude also suppresses the local unsteady pressure difference increase at 45% chord for 3.5 and 5 deg of oscillation. Increased steady loading results in decreased unsteady pressure difference over the front half chord. The effects of oscillation amplitude and steady loading are also evident on the unsteady pressure difference phase. Over the front 40% chord, the phase is relatively constant for the 5- and 10-deg oscillation amplitudes, but linearly increase for the 3.5-deg oscillating amplitude. However, aft of 40% chord, the phase is affected by both the steady loading and oscillation amplitude.

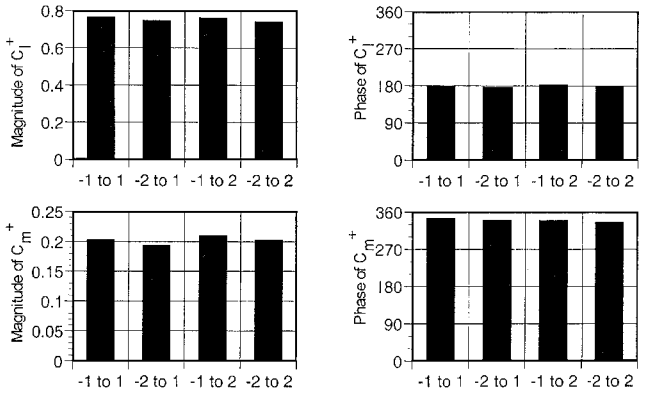

Fig. 9 Effect of influence terms on unsteady lift and moment.

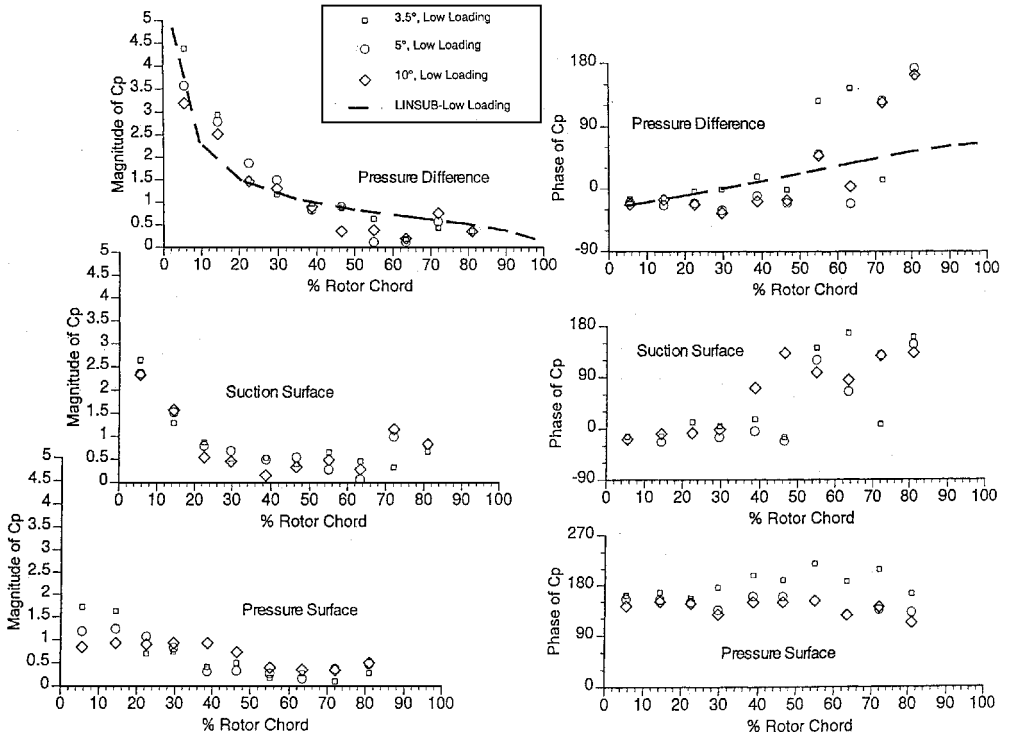

Fig. 10 Equivalent all-airfoils-oscillating unsteady pressure data at low steady loading.

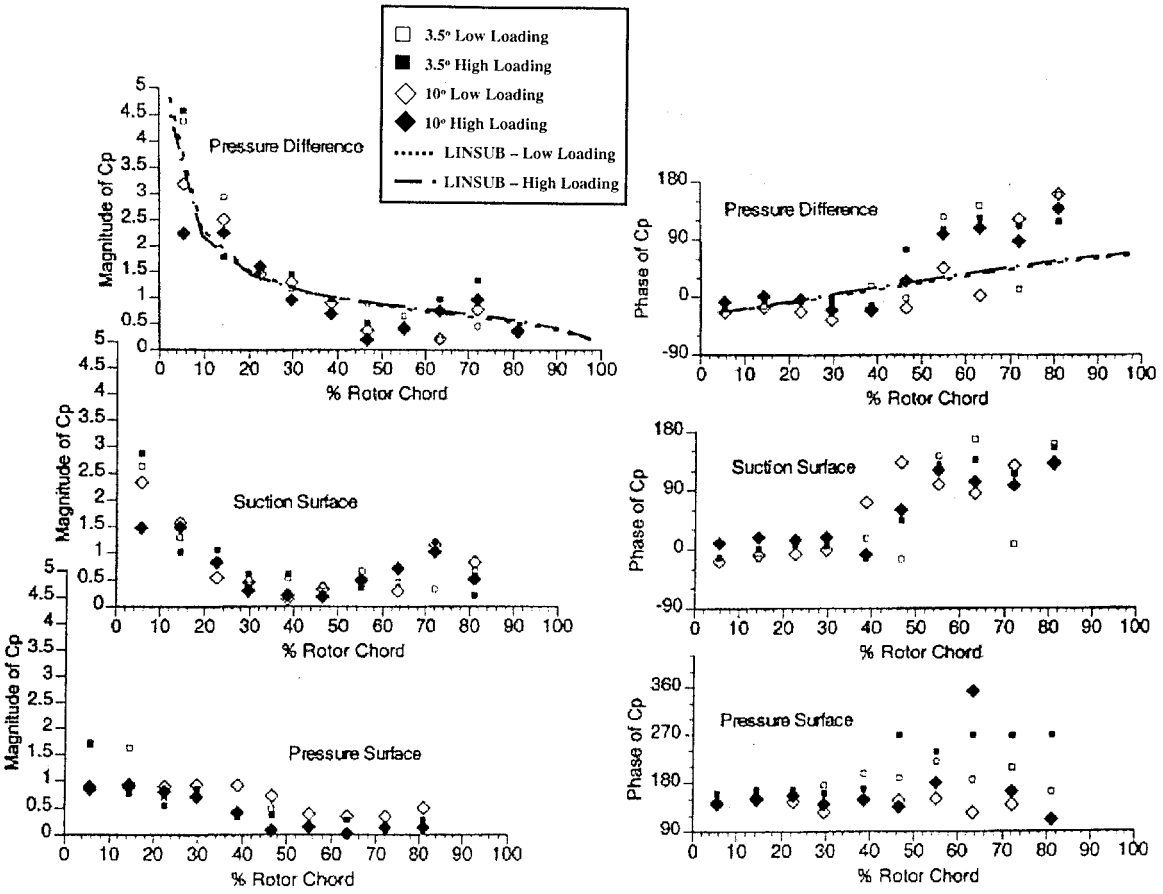

Fig. 11 Equivalent all-airfoils-oscillating unsteady pressure data at high steady loading.

Figures 10 and 11 also show the correlation of the 3.5-, 5-, and 10-deg oscillation amplitude, all-airfoil-oscillating data with LINSUB predictions for low and high steady loading. Note that in perturbation analyses such as this, the magnitude of the unsteady aerodynamics is linearly proportional to the oscillation amplitude. Hence, there is only one prediction for all three oscillation amplitudes at a particular steady loading. The unsteady pressure difference data generally correlate well with LINSUB in trend, but a higher decrease in magnitude is predicted along the front half chord and a lower decrease in magnitude over the aft chord region. The large shift in the phase data over the aft chord region is not predicted. Overall, the 3.5-deg oscillation amplitude data at low steady loading correlate the best. However, the chordwise magnitude and phase data do not match the predictions because, even at low steady loading with small perturbations, the rotor blade camber causes steady lift that is not considered.

First Harmonic Unsteady Lift and Moment Coefficients

The linearity of the oscillating airfoil unsteady aerodynamics is addressed by considering the effect of oscillation amplitude on the unsteady lift and moment at low steady loading. The phase of the lift and moment influence coefficients should be constant with oscillation amplitude because it is nondimensionalized by the complex blade motion. The magnitudes of the lift and moment coefficients are nondimensionalized by the rotor relative dynamic pressure only and, thus, should increase linearly with increasing oscillation amplitude $\bar{\alpha}$, as indicated by a linear reference line extended from zero oscillation amplitude to the low oscillation amplitude data.

Figure 12 shows the effect of oscillation amplitude on the first harmonic unsteady lift influence coefficient magnitude and phase. For blade $n = 0$ oscillating, the phase data are relatively constant as the oscillation amplitude is increased, in agreement with linear theory. With blades in other positions oscillating, the unsteady lift phase data shifts 30 deg or less between the 3.5- and 5-deg oscillation amplitudes, but is relatively constant between the 5- and 10-deg oscillation amplitudes. However, the lift magnitude data exhibit different behavior. The 5- and 10-deg oscillation amplitude lift influence coefficients are consistently smaller than the linear magnitude reference line extended from the 3.5-deg oscillation amplitude, except at low values of lift magnitudes for blades oscillating in positions $n = -2$ and 1. The $n = -2$ oscillating blade influence magnitude data are linear for all oscillation amplitudes. Also, summing the influence coefficients from blades $n = -2$ to 1 for lift, the nonlinearities in the influence coefficients magnitudes offset one another, with the equivalent all-airfoils-oscillating unsteady lift magnitudes deviating less from the linear line extended from the 3.5-deg oscillation amplitude. Clearly, nonlinear response is encountered for blades

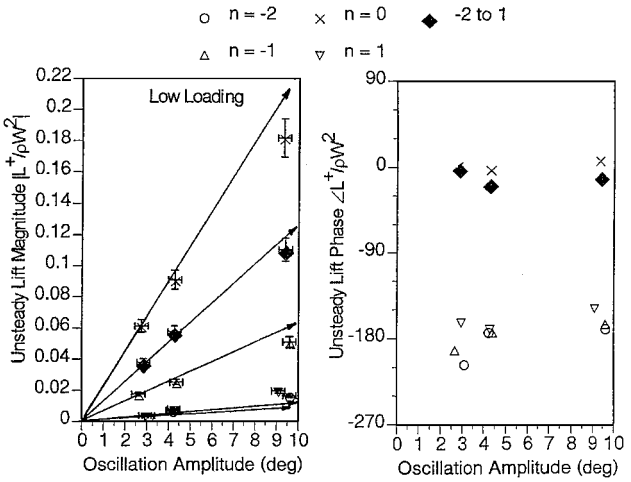

Fig. 12 Oscillation amplitude effect on unsteady lift.

oscillating at amplitudes larger than 5 deg. Note that, although the influence coefficient technique is linear, nonlinear unsteady aerodynamic effects are captured in the experiments, that is, the influence coefficient technique is fundamentally a Fourier transform analysis of nonlinear data and, as such, does not linearize the data.

The effect of oscillation amplitude on the equivalent all-airfoils-oscillating blade row first harmonic instantaneous lift coefficients variation with instantaneous incidence is presented in Fig. 13. The unsteady magnitude and phase effects are evident at the same time, with the area of the instantaneous lift-incidence curves corresponding to the magnitude and the ellipse skewness the phase. The arrows on the individual loops indicate the direction of time. For linear unsteady aerodynamics, the smaller oscillation amplitude data would be enclosed within the larger oscillation amplitude results, with the loop size proportionally larger with increased oscillation amplitude. Clearly, the oscillation amplitude affects both the equivalent all-airfoils-oscillating first harmonic lift data magnitude and phase. Also, the first harmonic unsteady lift data are not linear at an oscillation amplitude of 10 deg.

Higher Harmonic Unsteady Aerodynamics

Figure 14 presents the variation with instantaneous incidence of the sum of five harmonics of the instantaneous lift coefficients. Because the blade motion is essentially a first harmonic motion, the sum of the five harmonics of the instantaneous lift data being significantly different from the first harmonic implies that the oscillating airfoil unsteady aerodynamics are nonlinear, that is, higher harmonics are significant. Also, the five-harmonic instantaneous lift loops are very different from one another at the three oscillation amplitudes.

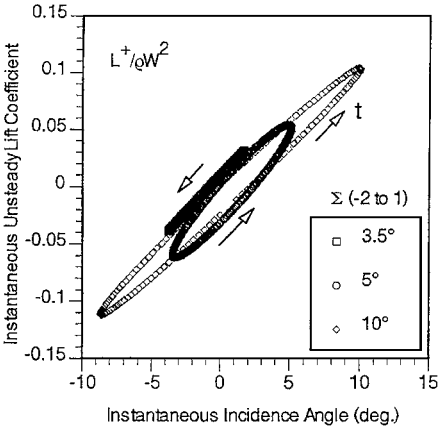

Fig. 13 Equivalent all-airfoils-oscillating first harmonic instantaneous lift with incidence.

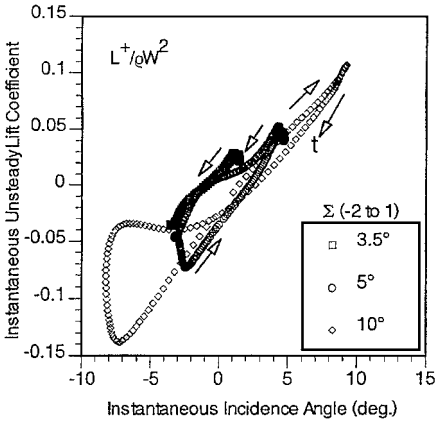

Fig. 14 Equivalent all-airfoils-oscillating instantaneous lift variation with incidence, five harmonics summed.

Summary and Conclusions

Experiments were performed directed at investigating and quantifying the aerodynamic damping unsteady aerodynamics of the first-stage rotor of a research compressor, including the effects of oscillation amplitude and steady aerodynamic loading. The resulting rotor blade aerodynamic damping oscillating airfoil data were then correlated with a linear theory prediction.

In general, the unsteady pressure influence coefficient data decayed rapidly with increasing distance from the reference blade, with the influences different on the pressure and suction surfaces. Significant effects of oscillation amplitude and steady loading were evident on the influence coefficient data, as well as the equivalent all-airfoils-oscillating unsteady pressure data.

Equivalent all-airfoils-oscillating unsteady pressure data were obtained by summing the influence coefficient data for blades $n = -2$ to 1 oscillating. Although oscillation amplitude effects were evident on both blade surfaces, it had a larger effect on the pressure surface magnitude. Steady loading had a significant effect on all of the equivalent all-airfoils-oscillating unsteady pressure data. In general, increased oscillation amplitude and increased steady loading resulted in reduced unsteady pressure response magnitude and larger chordwise phase data shifts. Correlation with LINSUB predictions was relatively good. However, the chordwise magnitude and phase unsteady pressure difference data did not match the predictions because this classical linear theory does not account for blade camber or steady loading.

Analysis of the unsteady lift harmonics indicated a nonlinear response in the oscillating blade row unsteady aerodynamics for oscillation amplitudes greater than 5 deg. The unsteady lift from individual blade oscillations exhibited a more nonlinear response, which when summed to compute the equivalent oscillating blade row unsteady lift showed an extended linear response region. The nonlinear response resulted in a decreased first harmonic unsteady lift at the higher oscillation amplitudes. These results indicate that performing a first harmonic analysis may not be sufficient to determine oscillating airfoil aerodynamics for flutter and forced response at high amplitudes of oscillation because significant, higher harmonic, nonlinear effects might be neglected.

Acknowledgments

This research sponsored, in part, by the Army Research Office. This support is most gratefully acknowledged. The truly exceptional design and manufacturing support from R. D. McGuire is also gratefully appreciated and acknowledged.

References

[1] Buffum, D. H., and Fleeter, S., "Oscillating Cascade Aerodynamics by an Experimental Influence Coefficient Technique," *Journal of Propulsion*, Vol. 6, No. 5, 1990, pp. 612–620.

[2] Buffum, D. H., and Fleeter S., "Wind Tunnel Wall Effects in a Linear Oscillating Cascade," *Journal of Turbomachinery*, Vol. 115, No. 1, 1993, pp. 147–156.

[3] Hardin, L. W., Carta, F. O., and Verdon, J. M., "Unsteady Aerodynamic Measurements on a Rotating Compressor Blade Row at Low Mach Number," American Society of Mechanical Engineers, ASME Paper 87-GT-221, June 1987.

[4] Verdon, J. M., and Caspar J. R., "Subsonic Flow Past an Oscillating Cascade with Finite Mean Flow Deflection," *AIAA Journal*, Vol. 18, No. 5, 1980, pp. 540–548.

[5] Henderson, G. H., and Fleeter, S., "Oscillating Aerodynamics and Flutter of an Aerodynamically Detuned Cascade in an Incompressible Flow," *International Journal of Turbo and Jet Engines*, Vol. 10, No. 4, 1993, pp. 135–154.

[6] Whitehead, D. S., "Classical Two-Dimensional Methods," AGARDograph 298, *AGARD Manual on Aeroelasticity in Axial Flow Turbomachines, Volume 1: Unsteady Turbomachinery Aerodynamics*, 1987, pp. 3.1–3.30.